Thin Solid Films 648 (2018) 21–25

Contents lists available at ScienceDirect

Thin Solid Films

journal homepage: www.elsevier.com/locate/tsf

Estimation of residual stresses in perovskite films for capacitor applications

E. Ramos-Moore[a,b,*], P. Leibenguth[b,c], S. Slawik[b], R.S. Coelho[d], D. Horwat[e], S. Migot[e], B. Lechthaler[b], F. Mücklich[b]

[a] Facultad de Física, Pontificia Universidad Católica de Chile, Santiago 7820436, Chile
[b] Universität des Saarlandes, Functional Materials, Campus D3.3, D-66123 Saarbrücken, Germany
[c] Plansee SE, 6600 Reutte, Austria
[d] Departamento de Materiais, SENAI — CIMATEC, Av. Orlando Gomes 1845, Piata, Salvador, BA 41650-010, Brazil
[e] Institut Jean Lamour, UMR7198, Université de Lorraine, 54011 Nancy, France

ARTICLE INFO

Keywords:
X-ray stress analysis
Texture analysis
Platinum electrode
Perovskites
Thin films
Lead zirconate titanate

ABSTRACT

The performance of perovskite films in capacitor devices is strongly determined by the level of residual stresses developed after their fabrication at high temperatures. Quantification of these stresses by X-ray diffraction is not straightforward in perovskite films due to the complexity of the crystalline structure and a lack of effective elastic diffraction constants. In this work we apply a simple and accurate method to estimate the residual stresses developed in $Pb(Nb,Zr,Ti)O_3$ perovskite films grown by metal–organic chemical vapor deposition on the Pt electrode. The stress was directly measured in the Pt bottom electrode film before and after the deposition of the perovskite film and compared with intrinsic and thermal stresses calculations. Our results reveal in-plane tensile stresses of 676(8) MPa developed in the Pt electrode, which mainly originate from the relative thermal contraction between $Pb(Nb,Zr,Ti)O_3$ and Pt as well as the cubic-tetragonal perovskite phase transformation after deposition. This methodology is straightforward and highlights the possibility to perform systematic studying for tailoring stress conditions and improving the performance of perovskite films for capacitor applications.

1. Introduction

Capacitors based on perovskite lead zirconate titanate – $Pb(Zr,Ti)O_3$ – (PZT) thin films are currently used in non-volatile memories and optoelectronics devices due to their property of retaining and switching electric polarization [1]. The study and further tailoring of strains within the capacitors multilayer are crucial to develop high-performance devices [2]. In particular, several works have reported the effect of the substrate layer and the film thickness on the microstructural [3–8], piezoelectric [9–11], ferroelectric [12–15] and optical [16,17] properties of PZT. At room temperature, PZT exhibits a tetragonal structure, which defines two types of ferroelectric regions at the surface: *a* and *c* domains [2]. It has been found that the increase of *a*-domains fraction and film thickness yields a drop of the piezoelectric and ferroelectric properties due to the intrinsic relaxation of stresses in the multilayer. These effects are associated mainly to anisotropic strains that arise at the film/substrate interface [18]. In most of the referred works, quantitative strain measurements have been carried out by X-ray diffraction (XRD) using the broadening of Bragg-peaks, which is usually limited in their interpretation, since inhomogeneous grain size, experimental broadening and crystallographic texture can also affect the peak width and therefore the determination of microstrains [19]. Moreover, absolute values of stresses estimated in PZT-based films from strain measurements are not straightforward mainly due to the complex tetragonal symmetry with a c/a ratio close to 1 and a lack of information regarding the diffraction elastic constants at room and high temperatures.

In this work, we apply a simple and accurate method to estimate residual stresses in perovskite niobium-doped lead zircomate titanate – $Pb(Nb,Zr,Ti)O_3$ – (PNZT) grown on Pt electrodes by metal–organic chemical vapor deposition (MOCVD) [20,21]. In particular, we estimate the stress in Pt using X-ray stress analysis (XSA) through the $\sin^2\psi$ method and compare with calculated values by considering different strain sources [19]. The microstructure and crystallinity of the multilayer system is analyzed by scanning transmission electron microscopy (STEM) and transmission electron microscopy (TEM). Substrates (Pt/substrate) and samples with the top perovskite film (PNZT/Pt/substrate) were subjected to the same thermal and pressure conditions in order to study the effects of the film deposition process. Since PNZT is partially transparent to X-rays, three Bragg reflections of Pt were accessible to perform strain/stress and texture analyses.

* Corresponding author.
E-mail address: evramos@fis.puc.cl (E. Ramos-Moore).

https://doi.org/10.1016/j.tsf.2018.01.011
Received 2 October 2017; Received in revised form 13 December 2017; Accepted 7 January 2018
Available online 08 January 2018

2. Methods

The samples of this work were provided by Radiant Technologies Inc. and consisted of 4 wt% of Nb doped $Pb(Zr_{0.2}Ti_{0.8})O_3$ thin films (≈900 nm) grown at 650 °C MOCVD on the following substrate: Pt (≈150 nm)/TiO_2 (≈50 nm)/SiO_2 (≈500 nm)/Si. STEM and TEM lamella preparation were performed using a dual-beam focused ion beam/scanning electron microscopy (FIB/SEM) workstation (FEI Helios NanoLab 600), whereas TEM diffraction was performed using Philips CM200 TEM microscope operated at 200 keV. XRD phase analysis was performed in a PANalytical MPDpro system using Cu$K\alpha_1$-radiation (1.5406 Å) with parallel incident/diffracted beam optics and symmetrical θ-θ geometry. Texture and XSA measurements were carried out in a PANalytical MRD system using Cu$K\alpha$-radiation (1.5418 Å) with parallel incident/diffracted beam optics. The d-sin$^2\psi$ curves were obtained by measuring 2θ-scans (0.02° step size and 10 s acquisition time) and varying ψ from 0° to 80°, which corresponds to an irradiated area between 10.8 mm^2 and 39.3 mm^2. Deconvolution and fitting of the X-ray reflection peaks were performed using linear background subtraction and Voigt profile functions. Therefore, all the plotted values of the d-spacing include the statistical error bar. Negative values of ψ were not considered because neither Pt nor PNZT showed shear strains in preliminary measurements. Pole figures were measured by integrating the intensity of selected Pt reflections within a $2\theta = 1°$ range at fixed 2θ angles and 10 s acquisition time. The experiments were conducted covering the φ range from 0° to 360° and the ψ from 0° to 85° with 5° step size. Here, three linearly independent reflections of Pt were measured Pt 111, Pt 311 and Pt 420. The complete pole figures were calculated through the orientation distribution functions (ODF) using the standard software LaboTex®.

3. Results and analysis

The microstructure from a multilayer cross section and selected area electron diffraction (SAED) pattern from the PNZT film are displayed in Fig. 1. STEM micrograph shows the PNZT/Pt/TiO_x/SiO_x/Si system, where the layers, and oxide interfaces are detected by the different image contrasts. The TiO_x/SiO_x interface shows a higher roughness as compared with the PNZT/Pt interface. The indexed diffraction spots of the SAED pattern obtained from the indicated zone reveals a PNZT film composed by textured grains with a preferred orientation of type ⟨110⟩. As shown in Fig. 1, the thickness of the PNZT layer is close to 1 μm, and the white points observed in the PNZT layer correspond to voids that are slightly richer in oxygen due to local differences in temperature and partial pressure of oxygen during deposition.

X-ray diffraction patterns measured on Pt/substrate and PNZT/Pt/substrate at RT are shown in Fig. 2. The Pt lattice constant estimated in Pt/substrate by the Nelson-Riley (NR) method [22] was $a_{Pt} = 3.914(1)$ Å (3.923 Å in bulk [23]). The Pt reflections: Pt 111 (39.74°), Pt 311 (81.66°) and Pt 420 (123.61°) were observed in both samples and were used to perform the texture and strain analyses. In addition, sample containing the PNZT film reveal additional tetragonal reflections [24]: PNZT 100 (22.26°), PNZT 110 (31.59°), PNZT 111 (38.94°), PNZT 200 (45.50°), PNZT 210 (51.08°) and PNZT 211 (56.28°). The a- and c-domains (inset in Fig. 2) correspond to 100 and 001 reflections of PNZT, respectively. The small peaks not designated in Fig. 2 correspond to titanium-based compounds. The following a and c lattice constants of tetragonal PNZT (TE) were estimated by NR: a_{TE} 3.990(2) Å and c_{TE} 4.060(2) Å. Whereas the tetragonality of the film was $[c - a]/a = 0.018(1)$, which agrees with values measured [12,25] in similar systems. By comparing the area of the deconvoluted a-(PNZT 100) and c-(PNZT 001) domain peaks of PNZT shown in Fig. 2, a volume fraction of the c-domains $\alpha_c = 0.4$ was estimated, which suggests the formation of a metastable $a/c/a/c$ phase [2]. The averaged grain size of PNZT estimated from Scherrer equation is close to 10 nm. In terms of X-ray absorption, the PNZT layer acts as a filter that produces a decrease of the Pt peaks intensity (see Fig. 2).

In order to former estimate residual stresses developed in the PNZT layer after their deposition through MOCVD growth, reflections 110 and 111 of the PNZT phase were chosen to apply the sin$^2\psi$ method. As observed in Fig. 3, d-sin$^2\psi$ distributions measured in the PNZT layer show strong non-linear behavior in both reflections. This behavior is usually attributed to micro-plastic deformation, concentration gradients and strong texture, and does not allows to apply the linear equation of XSA in order to directly estimate the stress [19]. In particular, the shape of the d-sin$^2\psi$ distributions for PNZT 111 suggests the generation of a stress depth gradient due to the fact that border conditions impose zero stress at the top of the PNZT layer, whereas none-zero stress state at the bottom interface.

Recalculated pole figures of Pt 111, Pt 311 and Pt 420 reflections measured on Pt/substrate and PNZT/Pt/substrate samples are shown in Fig. 4. A ⟨111⟩ fiber-texture of Pt is observed in both samples. Rings observed in Pt 111 at around $\psi = 70°$ correspond to permutations of 111 reflections; in Pt 311 at around $\psi = 30°$ and 60° correspond to the angles between ⟨311⟩ and ⟨111⟩; and in Pt 420 at around $\psi = 40°$ and 75° correspond to the angles between ⟨420⟩ and ⟨111⟩. The texture analyses indicate that the deposition of PNZT onto Pt/substrate does not affect the orientation of the Pt layer. Moreover, the presence of PNZT film increases the X-ray absorption, decreasing the texture strength.

The d-sin$^2\psi$ curves of Pt 111, Pt 311 and Pt 420 reflections measured on Pt/substrate and PNZT/Pt/substrate samples are summarized in Fig. 5. The analyses reveal that all curves obtained from Pt/substrate in the Pt layer show non-linear behavior. Since *hhh* reflections in cubic materials are not affected by texture-induced elastic film anisotropy and should exhibit linear behavior [26], our most plausible explanation for the non-linear behavior observed for the Pt 111 reflection measured on the Pt/substrate sample (see Fig. 5) is the elastically anisotropic

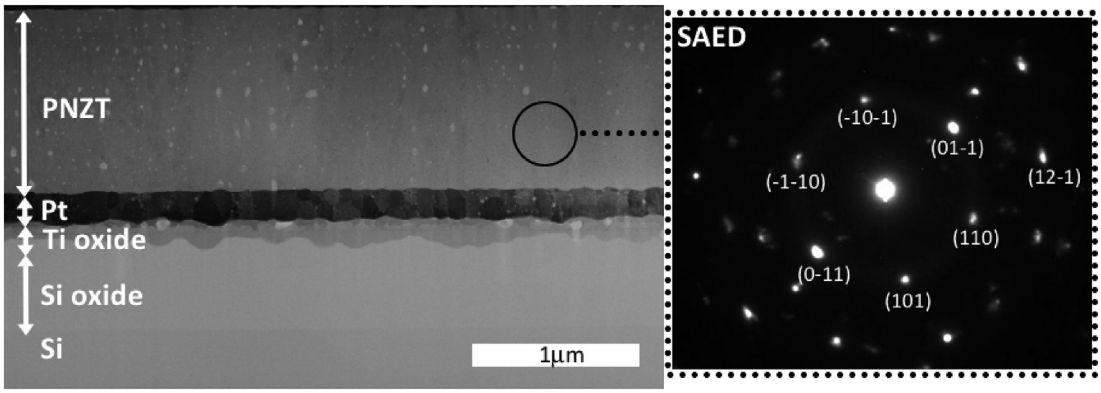

Fig. 1. Left: STEM image of the multilayer system PNZT/Pt/substrate. Right: Selected area electron diffraction (SAED) of the PNZT layer showing local preferred ⟨110⟩ orientation.